ENHANCING THE EFFICIENCY OF CEMENT-BASED TRIBOELECTRIC NANOGENERATORS THROUGH OPTIMIZED ELECTRODE CONFIGURATIONS

Kanisorn Kaewsrithong[1,2], Ruamporn Potong[3], Rattiyakorn Rianyoi[4,5], Watcharapong Wongkeo[6], Pincha Torkittikul[7], Chatdanai Boonruang[4,5], Arnon Chaipanich[4,5], Panisara Disuea[1,2], Anucha Kaewpoonsuk[1,2] and Thanongsak Nochaiya[1,2,*]

Received: September 02, 2024; Revised: February 09, 2025; Accepted: February 11, 2025

Abstract

Cement-based materials, commonly used in construction, show great potential as triboelectric nanogenerators. However, the electrode type for cement-based triboelectric nanogenerators (CTENGs) significantly influences not only the electrical output but also the durability of the device. Therefore, this study aims to investigate the effects of electrode type and the distance between the electrode and the sample surface on the electrical output performance of CTENG. The CTENG with stainless steel plate and wire mesh electrodes was evaluated in a vertical contact-separation mode. The results revealed that the wire mesh electrode not only improved the electrical output but also enhanced the durability of the CTENG compared to the plate electrode. Additionally, greater open-circuit voltage and short-circuit current values were obtained by decreasing the distance between the electrode and the sample surface. At distance of 1 mm, the CTENG achieved a power density of up to 139 mW/m² when connected to an external load of 10 MΩ. This study offers a promising strategy to enhance the performance and durability of CTENGs, enabling their efficient use as energy-harvesting materials.

Keywords: **Cement paste; Electrode; Energy harvesting; Triboelectric nanogenerator**

---

[1] *Department of Physic, Faculty of Science, Naresuan University, Phitsanulok 65000, Thailand. E-mail: kanisornka65@nu.ac.th; jeerapad@nu.ac.th; anuchak@nu.ac.th; thanongsakno@nu.ac.th[*]*
[2] *Research Center for Academic Excellence in Applied Physics, Naresuan University, Phitsanulok 65000, Thailand.*
[3] *Division of Physics, Faculty of Science and Technology, Rajamangala University of Technology Thanyaburi, Pathum Thani, 12110, Thailand. E-mail: ja.ruamporn@gmail.com*
[4] *Department of Physics and Materials Science, Faculty of Science, Chiang Mai University, Chiang Mai 50200, Thailand. E-mail: r.rianyoi@gmail.com, arnonchaipanich@gmail.com*
[5] *Center of Excellence in Materials Science and Technology, Chiang Mai University, Chiang Mai 50200, Thailand. E-mail: chatdanaiboonruang@gmail.com*
[6] *Physics and General Science Program, Faculty of Science and Technology, Nakhon Ratchasima Rajabhat University, Nakhon Ratchasima 30000, Thailand. E-mail: watcharapong_l@hotmail.com*
[7] *Department of Civil Technology, Faculty of Industrial Technology, Lampang Rajabhat University, Lampang, 52100, Thailand. E-mail: pincha_t@g.lpru.ac.th*
[*] *Corresponding author*

DOI: https://doi.org/10.55766/sujst11182

Introduction

Global interest in mechanical energy harvesting has grown significantly, with triboelectric nanogenerators (TENGs) standing out as a key innovation notable advantages of TENGs include high power output, superior efficiency, affordable fabrication, and simple production procedures. TENGs are capable of harvesting mechanical energy from environmental sources such as human motion, vibrations, or vehicle movements and converting it into electrical energy. The working principle of TENGs is based on two phenomena: triboelectrification and electrostatic induction (Zhou *et al*., 2020). TENGs are typically fabricated from two distinct materials, which, upon contact, undergo surface charge transfer. When the two materials are subsequently separated, the induced charges generate an electric current. However, the electrical output of TENGs is significantly influenced by the dielectric constant of the materials used (Kim *et al*., 2017). Enhancing the dielectric constant can be achieved by incorporating filler materials into the primary matrix. These filler materials are categorized into two types: high-dielectric constant fillers such as TiO_2, $BaTiO_3$, $SrTiO_3$, or Ta_2O_5 (Chen *et al*., 2016; Kim *et al*., 2017; Kang *et al*., 2020; Bunriw *et al*., 2021;), and conductive fillers such as silver nanoparticles (Ag), carbon black, carbon nanotubes, and graphite (Wang *et al*., 2016; Choi *et al*., 2021; Suphasorn *et al*., 2021). Additionally, the electrical output of TENGs is enhanced by surface polishing (Kaewsrithong *et al*., 2023) and modification of dielectric material surfaces by designed contact patterns (Kisomi *et al*., 2024). However, although this issue has not been extensively studied, changes to the electrode configuration can also improve the performance of TENGs (Yoo *et al*., 2019).

Cement, a fundamental material in construction, is constantly subjected to mechanical forces, both static and dynamic. When hardened, cement exhibits excellent compressive strength, durability, and the ability to form various shapes.Reports have demonstrated the use of cement as a base material in cement-based triboelectric nanogenerators (CTENGs). By adding additives such MXenes, the power generation capabilities of these devices are increased by 86% and the electrical output is significantly increased by about twice compared to pristine CTENG (Palaniappan *et al*., 2023). The additional of TiO_2 (Sintusiri *et al*., 2020) and carbon black (Kuntharin *et al*., 2022) have been shown to achieve maximum power densities of 0.265 W/m^2 and 2.38 W/m^2, respectively. This study recommended that a stainless-steel sheet used as the electrode for CTENGs be positioned more than 7.5 mm apart from both cement surfaces to prevent the sample cracking from the mechanical press during the TENG performance test (Kuntharin *et al*., 2022). Additionally, cement is known to possess a high positive tribo-charge, as it is a mineral-based material similar to glass and ceramics, according to the triboelectric series (Kim *et al*., 2017; Yu *et al*., 2019). However, since cement is a non-conductive substance, electrodes are necessary to enable electron transit in the system while evaluating CTENGs performance in a contact-separation mode. Moreover, the long-term stability of metallic electrodes can be affected by corrosion due to the high alkalinity (pH of approximately 13) of hardened cement. Selecting appropriate electrodes that are resistant to corrosion and capable of withstanding compressive forces is crucial for achieving optimal CTENGs performance. In this study, electrodes comprise of stainless steel were used. Two electrode types-plate and wire mesh-were examined for efficacy. Additionally, the effect of the distance between the electrode and the test surface (the cement paste thickness) on the electrical output of the CTENGs was investigated. The findings aim to develop sustainable energy-harvesting materials by identifying the optimal parameters, particularly the cement thickness and electrode type, for C-TENG design.

Materials and Methods

In this investigation, 5×5 cm^2 acrylic molds were used to cast cement paste specimens. To study the effect of electrode type, plate and wire mesh electrodes with a 1,000-micrometer mesh size, made of stainless steel to resist corrosion during cement hydration reactions, were utilized. To create a consistent paste, Portland cement Type I was manually mixed with water for around five minutes, maintaining the water-to-cement ratio at 0.3 by weight. A 4×7 cm^2 electrode was positioned in the center of the mold, 1 cm beyond each side of the specimen, after the first 0.5 cm-thick layer of cement paste had been poured. After carefully removing any air bubbles, a second layer of cement was placed until the whole layer was 1 cm thick. Moreover, distances of 1, 2, 3, 4, and 5 mm between the sample surface and the wire mesh electrode were set to extensively investigate the effect of surface-electrode distance. All samples were then cured for 7 days under controlled relative humidity of approximately 95% before undergoing electrical output testing.

The electrical performance of CTENG was assessed in a vertical contact-separation mode with polytetrafluoroethylene (PTFE) as the grounded negative tribo-material and the cement paste with stainless-steel electrode as the positive electrode. Triboelectric charging occurred by pressing PTFE onto the composite surface at a frequency of 5 Hz and the contact force of 11 N. An oscilloscope (Tektronix TBS1052B) was used to measure open-circuit voltage (Voc) and power density across external resistances ranging from 1 to 100 MΩ. A digital ammeter (Keithley DMM6500) was used to record short-circuit current (Isc).

To investigate the specific characteristics and reactions of the cement, the prepared cement paste was immersed in acetone for 24 hours for stop the hydration reaction. After that, the samples were dried in an oven at 60°C for 48 hours. The specimen was then fractured into smaller pieces for morphological analysis using a field-emission scanning electron microscope (FE-SEM; Thermo Fisher APERO S). A section of the sample was ground to approximately 100 micrometers in order to crystal structure analysis using X-ray diffraction (XRD; Bruker D2PHASER) techniques. Additionally, a disc-shaped sample (11 mm in diameter and 2 mm thick) was prepared for dielectric property testing. After 7-days curing, the paste sample was oven-dried at 100°C for 24 hours to remove moisture in the samples, and then coated both surfaces with low-temperature conductive silver paint for electrode preparation. The dielectric properties of the cement paste were measured using a Keysight E4980A Precision LCR Meter at room temperature.

Results and Discussion

Characterization of CTENG

The microstructural characteristics of cement powder and hydrated cement (cement paste) were investigated using scanning electron microscopy (SEM), and their crystalline phases were analyzed using X-ray diffraction (XRD), (as presented in Figures 1(a-c), respectively). The SEM micrograph of the raw cement powder (Figure 1(a)) revealed irregularly shaped particles with slight agglomeration (as seen in the small particles). The particle sizes were predominantly less than 100 µm, consistent with the typical size distribution of cement powder used in construction applications. Upon hydration (Figure 1(b)), significant changes in the microstructure were observed. The cement matrix exhibited a denser structure due to the formation of calcium silicate hydrate (C-S-H) phases (fibrous-liked structure as presented in the insight), calcium hydroxide, and ettringite. These hydration products play a crucial role in binding the cement particles together, contributing to the strength development and durability of the material (Akkarapongtrakul *et al*., 2017). However, bubbles (indicated by arrows in Figure 1b) were also observed. These features are likely artifacts resulting from the sample preparation process during mixing and compacting.

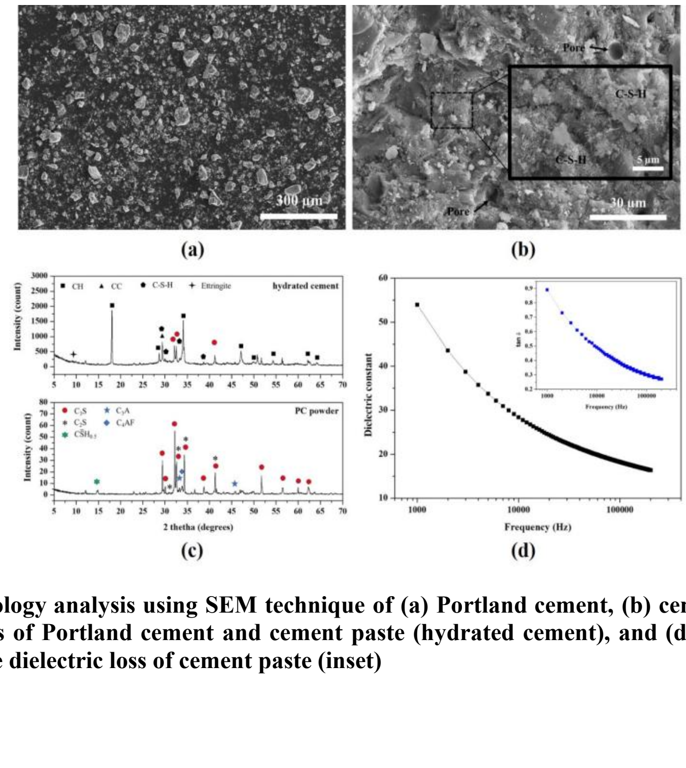

Figure 1. Morphology analysis using SEM technique of (a) Portland cement, (b) cement paste, (c) XRD patterns of Portland cement and cement paste (hydrated cement), and (d) dielectric constant with the dielectric loss of cement paste (inset)

The XRD pattern of the cement powder revealed the presence of primary crystalline phases, including tricalcium silicate (C_3S) and dicalcium silicate (C_2S), tricalcium silicate (C_3A) and tetracalcium aluminoferrite (C_4AF) which are the main contributors to strength development in cement. Additionally, minor phases such as calcium sulfate hydrate were detected, consistent with typical cement compositions (Gonçalves *et al*., 2023). After hydration, the significant changes in the crystalline structure were observed. The XRD patterns of cement paste (Figure 1(c)) corroborate the SEM findings. The diffraction peaks confirmed the presence of key hydration products such as C-S-H, portlandite ($Ca(OH)_2$), and ettringite, along with residual unhydrated clinker phases. The intensity and sharpness of these peaks highlight the crystalline nature of the hydration products, contributing to the structural integrity of the hardened cement paste (Gonçalves *et al*., 2023; Hoshino *et al*., 2006).

The dielectric properties of the cement paste were measured at room temperature by various frequency, as presented in Figure 1(d). The results indicated that the dielectric constant and dielectric loss decreased with increasing testing frequency, a trend commonly observed in dielectric materials. The frequency-dependent behavior of the dielectric constant can be attributed to the polarization mechanisms in the cement paste. At low frequencies, dominant dipolar and interfacial polarization result in higher dielectric constants, while increasing frequency reduces these effects, causing a decline in the dielectric constant. This behavior aligns with the hydration process, where hydration products like C-S-H and portlandite significantly impact dielectric properties (Xin *et al*., 2007). At a frequency of 1 kHz, the dielectric constant and dielectric loss values were approximately 55 and 0.9, respectively. These values correspond to previous studies, which reported dielectric constant and dielectric loss values of cement paste of about 20-40 and 0.6-1.5, respectively (Sintusiri *et al*., 2020; Kuntharin *et al*., 2022). However, the dielectric properties of the cement paste vary depending on the water-to-cement ratio, admixtures and moisture content (Yu, 2011; Wen and Chung, 2001; Rianyoi *et al*., 2021).

Effect of electrode types

The design of the electrode for the cement-based triboelectric nanogenerator (CTENG) using stainless steel in both sheet and wire mesh forms. The electrical performance of the CTENG was evaluated, as shown in Figure 2. The triboelectric mechanism of the CTENG, with cement acting as a positive triboelectric material, was tested in conjunction with polytetrafluoroethylene (PTFE), as a negative triboelectric material. During the contact-separation process, a negative charge (electrons) was induced to move into or out of the CTENG material due to electrostatic and electromagnetic induction phenomena, as illustrated in Figure 2. This mechanism demonstrates the generation of an electric output through the interaction of the triboelectric materials. The results

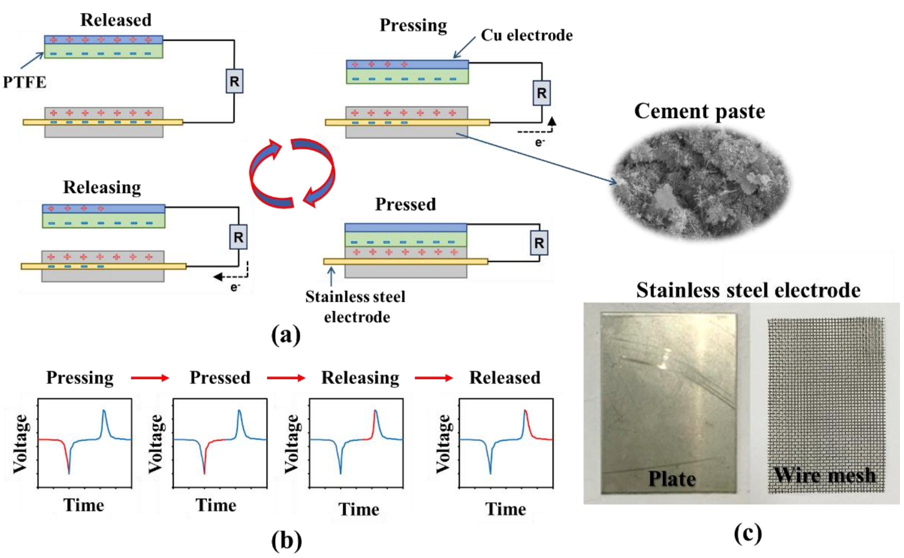

Figure 2. **(a) Schematic view of the working mechanism of CTENGs under a vertical contact-separation mode, (b) corresponding signal waveforms, and (c) photograph of the stainless steel plate and wire mesh**

confirm that the CTENG operates efficiently under the principles of triboelectric charging and charge induction, validating its potential for energy harvesting applications (Kuntharin *et al*., 2022; Sintusiri *et al.*, 2020).

As shown in Figure 3(a), the experimental results indicated that the CTENG with a wire-mesh electrode generated slightly higher electrical outputs, with an average peak-to-peak voltage (Vpp) of 22.5 V and a current (Ipp) of 13.0 µA, compared to 20.2 V and 12.45 µA for the plate electrode. Additionally, the findings supported with the power density results of the sample with wire-mesh electrode, reaching up to 6.5 mW/m^2 when connected to an external resistor of 10 MΩ while the CTENG with plate type electrode showed the power density peak of 5.2 mW/m^2, as presented in Figure 3b. However, the effect of modified electrode on the electrical output of TENG has been reported by Yoo *et al*. (2019) indicating that increasing the interfacial area between the dielectric layer and the electrode contributes to a higher capacitance of TENG, which enhances the tribo-charge density. Furthermore, the wire-mesh design contributes to stronger interfacial bonding with the cement paste, enhancing durability under compressive stresses and reducing the likelihood of interfacial cracking during mechanical testing.

Figure 4 demonstrates the superior performance and adhesion mechanism of the wire-mesh electrode compared to the plate electrode in cement-based triboelectric nanogenerators. The schematic view reveals that cement particles, with an average size smaller than 50 µm, bond to the mesh electrode through hydration products such as calcium silicate hydrate (C-S-H), calcium hydroxide (CH), and ettringite. These hydration phases form interconnected bridges across the mesh, effectively filling voids approximately 1000 µm in size, and ensuring robust adhesion to the electrode wires. The enhanced bonding strength is attributed to the chemical and mechanical interactions at the interface between the cement matrix and the mesh electrode.

Effect of electrode-to-surface distance

The effect of the electrode-to-surface distance on the electrical performance of the system was systematically investigated by varying the thickness of the cement paste layer encapsulating the electrodes from 1 mm to 5 mm. Stainless steel mesh electrodes with consistent dimensions (4 × 7 cm^2) were used (Figure 5(a)). The results demonstrated that the electrical output, both in terms of open-circuit voltage (*Voc*) and short-circuit current (*Isc*), exhibited a clear dependence on the distance between the electrode and the triboelectric interface.

The open-circuit voltage and short-circuit current results show consistent trends, as illustrated in Figures 5(b) and 5(c), respectively. It was

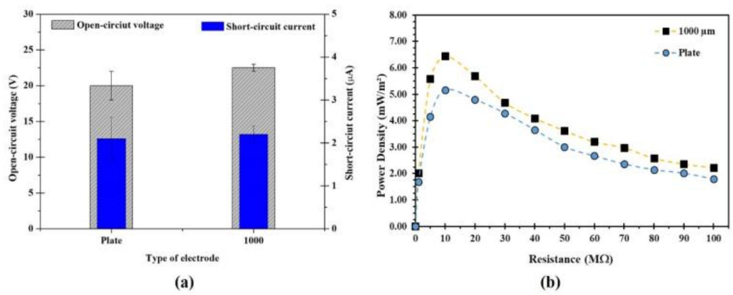

Figure 3. (a) Peak-to-peak voltage and current, and (b) power density of different electrode type (stainless steel plate and wire mesh)

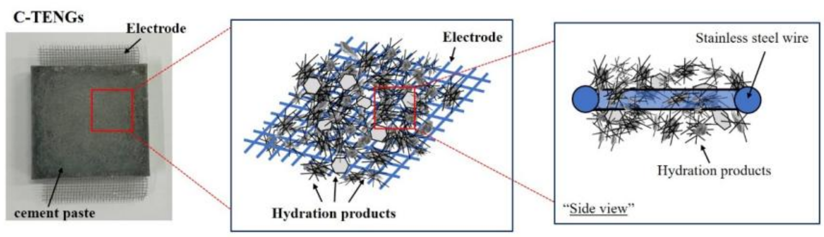

Figure 4. Schematic illustration of the interconnection of hydration products within the grids of the stainless-steel wire mesh (electrode), resulting in strong bonding to the wire mesh

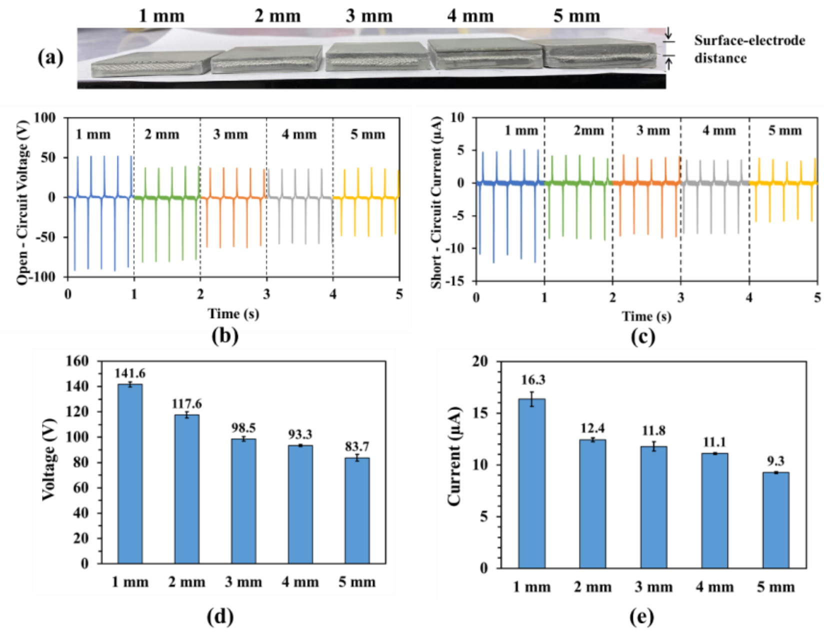

Figure 5. (a) A digital photograph of the CTENG with varying surface-to-electrode distances from 1 to 5 mm, and the electrical output measurements showing (b) Voc, (c) Isc, (d) peak-to-peak voltage, and (e) peak-to-peak current

observed that reducing the distance between the testing surface and the electrode led to a significant increase in the measured electrical outputs. Specifically, at electrode-to-sample surface distances ranging from 1 mm to 5 mm, the peak-to-peak voltage values were recorded as 141.6, 117.6, 98.5, 93.3, and 83.7 volts, respectively (Figure 5(d)). Similarly, the corresponding peak-to-peak current values were 16.3, 12.5, 11.8, 11.1, and 9.3 microamperes (Figure 5(e)). Additionally, when the maximum electrical outputs at the distance of 1 mm compared to those values at 5 mm, reaching to be higher by 1.69 and 1.76 times, respectively.

These findings highlight the critical role of tribo-charge in the performance of triboelectric systems. Charge induction strongly depends on the proximity of charge accumulation at the triboelectric interface to the electrode (tribo-charge density). The voltage (*V*) of TENG depends on many factors, including the distance between the electrode and the surface of materials (*d*), tribo-charge density (σ), dielectric constant of materials (ε_r), contract area (*S*), transfer charge (*Q*) and the distance between triboelectric materials, as described by equation 1 (Niu *et al*., 2013).

$$V = -\frac{Q}{S\varepsilon_0}\left(\frac{d_1}{\varepsilon_{r1}} + \frac{d_2}{\varepsilon_{r2}} + x(t)\right) + \frac{\sigma x(t)}{\varepsilon_0} \quad (1)$$

However, the open-circuit voltage (*Voc*) is investigated under conditions where there is no charge transfer (*Q* = 0), while the short-circuit current (*Isc*) represents the maximum current that can be generated when the voltage is zero (*V* = 0). These are described in equation 2 and equation 3, respectively (Niu *et al*., 2013).

$$V_{oc} = \frac{\sigma x(t)}{\varepsilon_0} \quad (2)$$

$$I_{sc} = \frac{S\sigma\left(\frac{d_1}{\varepsilon_{r1}}+\frac{d_2}{\varepsilon_{r2}}\right)v(t)}{\left(\frac{d_1}{\varepsilon_{r1}}+\frac{d_2}{\varepsilon_{r2}}+x(t)\right)^2} \quad (3)$$

According to these equations, both Voc and Isc depend on tribo-charge density, which is derived as a function of the distance between the electrode and the surface of a material. In this relationship, ε0 represents vacuum permittivity, d denotes the distance between the electrode and surface of triboelectric material, and ΔV is the potential drop of a TENG system, as following equation 4 (Harnchana *et al*., 2018).

$$\sigma = \frac{\varepsilon_0 \varepsilon_r \Delta V}{d} \quad (4)$$

It is noticed that the improvement of TENG performance relied on the electrode-to-surface distance. By decreasing this distance, the tribo-charge density increases, leading to higher open-circuit voltage and short-circuit current. Thus, minimizing the electrode-to-surface distance is a key factor in optimizing the energy conversion efficiency of TENG systems. This performance can be improved by adding materials with a higher dielectric constant and reducing the thickness of the electrification layer (Kang *et al*., 2020).

From Figure 6(a), the external resistance value that maximizes the power density was found by measuring the voltage drop across the resistors. The results demonstrated that the maximum power density of the CTENG reached 139 mW/m^2 and 33 mW/m^2 when coupled to an external resistance of 10 MΩ for samples with electrode-to-surface distances of 1 mm and 5 mm, respectively. These findings are consistent with the previously obtained electrical voltage and current results. Moreover, the power density behavior is consistent with the maximum power transfer theory (Plonus, 2020), which states that when the internal resistance and exterior resistance are equal, maximum power transfer takes place.

According to a study on a cement-based triboelectric nanogenerator's capacity for charge storage. This is achieved by utilizing a rectifier circuit (Figure 6(b)) to convert alternating current (AC) to direct current (DC) and then charging a 1 µF capacitor (Kaewsrithong *et al*., 2023). To compare electrode-to-surface distances of 1 mm and 5 mm, the voltage across the capacitor was measured (Sintusiri *et al*., 2020; Kuntharin *et al*., 2022; Kaewsrithong *et al*., 2023). The relationship between the voltage across the capacitor and the charging time exhibits an exponential trend. Initially, the voltage rises rapidly, reaching approximately 95% of its maximum value within about 30 seconds. The voltage across the 1 µF capacitor was 4.5 V for the sample with a 1 mm gap and 3.25 V for the sample with a 5 mm gap. Additionally, durability testing of the CTENG was conducted for prolonged operation over 5,000 cycles (Figure 6(c)). The results indicate a stable voltage output from the CTENG system, demonstrating its long-term operational reliability.

Conclusions

This study presents the significant impact of electrode type, surface-electrode distance, and hydration characteristics on the electrical performance and durability of CTENG. The wire-mesh electrode presented slightly increase electrical outputs compared to the plate electrode, reaching higher average peak-to-peak voltage and current, and also improved interfacial bonding with the cement paste. CTENG performance was significantly affected by the surface-electrode distance, with shorter distances leading to higher electrical outputs. The maximum voltage (141.6 V) and current (16.3 µA) were obtained at a distance of 1 mm from the electrode to the surface. The power density was 139 mW/m², demonstrating the efficiency of charge induction at closer distances.

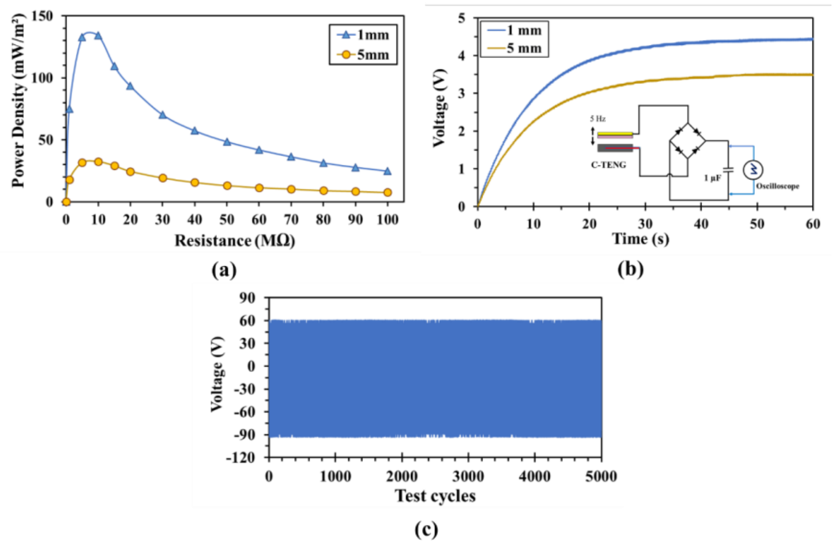

Figure 6. (a) Power density, (b) charging profile of 1 µF capacitors, a comparison of CTENG with surface-electrode distances of 1 mm and 5 mm, and (c) the performance of CTENG during over 5,000 cycles at 5 Hz with a contact force of 11 N.

Additionally, capacitor charging tests confirmed rapid voltage accumulation, with the CTENG achieving 95% of its maximum charge within 30 seconds while durability testing over 5,000 cycles revealed stable voltage outputs, showing the long-term reliability of the CTENG system. Overall, this study shows how wire-mesh electrodes in cement-based triboelectric systems can be used for energy harvesting applications by providing a balance between long-term dependability, high electrical performance, and structural integrity. The results offer an opportunity for improving CTENG designs to increase their effectiveness and variety in practical use.

Acknowledgement

The authors would like to express their gratitude to the Development and Promotion of Science and Technology (DPST) scholarship. This work was financially supported by Thailand Science Research and Innovation (TSRI) via Naresuan University under the Fundamental Fund’68 (Grant No. R2568B025). Additionally, this research work was partially supported by Faculty of Science, Naresuan University (Grant No. R2567E069). Moreover, we would like to thanks Global and Frontier Research University Fund, Naresuan University for all supports (Grant No.2567C001).

References

Akkarapongtrakul, A., Julphunthong, P., and Nochaiya, T. (2017). Setting time and microstructure of Portland cement-bottom ash-sugarcane bagasse ash pastes. Monatshefte für Chemie - Chemical Monthly, 148(8):1355-1362. https://doi.org/10.1007/s00706-017-1953-5

Bunriw, W., Harnchana, V., Chanthad, C., and Huynh, V.N. (2021). Natural rubber-TiO_2 nanocomposite film for triboelectric nanogenerator application. Polymers, 13(13):2213. https://doi.org/10.3390/polym13132213

Chen, J., Guo, H., He, X., Liu, G., Xi, Y., Shi, H., and Hu, C. (2016). Enhancing performance of triboelectric nanogenerator by filling high dielectric nanoparticles into sponge PDMS film. ACS Applied Materials & Interfaces, 8(1):736-744. https://doi.org/10.1021/acsami.5b09907

Choi, J.H., Ra, Y., Cho, S., La, M., Park, S.J., and Choi, D. (2021). Electrical charge storage effect in carbon-based polymer composite for long-term performance enhancement of the triboelectric nanogenerator. Composites Science and Technology, 207, 108680. https://doi.org/10.1016/j.compscitech.2021.108680

Gonçalves, B., Exposito, C., Ishikawa, T.T., and Koga, G.Y. (2023). X-ray diffraction study of the early hydration of Portland cements containing calcium carbonate by in-situ and ex-situ approaches. Construction and Building Materials, 365:129947. https://doi.org/10.1016/j.conbuildmat.2022.129947

Harnchana, V., Ngoc, H.V., He, W., Rasheed, A., Park, H., Amornkitbamrung, V., and Kang, D.J. (2018). Enhanced Power Output of a Triboelectric Nanogenerator using Poly(dimethylsiloxane) Modified with Graphene Oxide and Sodium Dodecyl Sulfate. ACS Applied Materials & Interfaces, 10(30):25263-25272. https://doi.org/10.1021/acsami.8b02495

Hoshino, S., Yamada, K., and Hirao, H. (2006). XRD/Rietveld Analysis of the Hydration and strength Development of Slag and Limestone Blended Cement. Journal of Advanced Concrete Technology, 4(3):357-367. https://doi.org/10.3151/jact.4.357

Kaewsrithong, K., Kaewpoonsuk, A., Torkittikul, P., Wongkeo, W., Chaipanich, A., Rianyoi, R., and Nochaiya, T. (2023). Boosting the electrical output of cement-based triboelectric nanogenerator by surface treatment technique. Journal of Physics: Conference Series, 2653:012052. https://doi.org/10.1088/1742-6596/2653/1/012052

Kang, X., Pan, C., Chen, Y., and Pu, X. (2020). Boosting performance of triboelectric nanogenerators by optimizing dielectric properties and thickness of electrification layer. RSC Advances, 10(30):17752-17759. https://doi.org/10.1039/D0RA02181D

Kim, Y.J., Lee, J., Park, S., Park, C., Park, C., and Choi, H.J. (2017). Effect of the relative permittivity of oxides on the performance of triboelectric nanogenerators. RSC Advances, 7(78):49368-49373. https://doi.org/10.1039/C7RA07274K

Kisomi, M.K., Roomi, M.S., and Mahmud, M.A.P. (2024). Mode-Adaptive Surface Pattern Design for Enhanced Triboelectric Nanogenerator Performance. Nanoenergy Advances. 4(4):328-343. https://doi.org/10.3390/nanoenergyadv4040020

Kuntharin, S., Harnchana, V., Klamchuen, A., Sinthiptharakoon, K., Thongbai, P., Amornkitbamrung, V., and Chindaprasirt, P. (2022). Boosting the Power Output of a Cement-Based Triboelectric Nanogenerator by Enhancing Dielectric Polarization with Highly Dispersed Carbon Black Nanoparticles toward Large-Scale Energy Harvesting from Human Footsteps. ACS Sustainable Chemistry & Engineering, 10(14):4588-4598. https://doi.org/10.1021/acssuschemeng.1c08629

Niu, S., Wang, S., Lin, L., Liu, Y., Zhou, Y.S., Hu, Y., and Wang, Z.L. (2013). Theoretical study of contact-mode triboelectric nanogenerators as an effective power source. Energy & Environmental Science, 6(12):3576-3583. https://doi.org/10.1039/c3ee42571a

Palaniappan, V., Adineh, A., Maddipatla, D., Bazuin, B.J., and Atashbar, M.Z. (2023). Development of an energy harvesting tile using novel MXene-cement based triboelectric nanogenerator. Proceedings of 2023 IEEE Sensors (pp. 1-4). Vienna, Austria. https://doi.org/10.1109/SENSORS56945.2023.10324981

Plonus, M. (2020). Circuit fundamentals. In Electronics and communications for scientists and engineers (2nd ed., Chap. 1). Butterworth-Heinemann. https://doi.org/10.1016/B978-0-12-817008-3.00001-2

Rianyoi, R., Potong, R., Ngamjarurojana, A., and Chaipanich, A. (2021). Mechanical, dielectric, ferroelectric and piezoelectric properties of 0-3 connectivity lead-free piezoelectric ceramic $0.94Bi_{0.5}Na_{0.5}TiO_3$-$0.06BaTiO_3$/Portland cement composites. Journal of Materials Science: Materials in Electronics, 32(4):4695-4704. https://doi.org/10.1007/s10854-020-05207-4

Sintusiri, J., Harnchana, V., Amornkitbamrung, V., Wongsa, A., and Chindaprasirt, P. (2020). Portland Cement-TiO2 triboelectric nanogenerator for robust large-scale mechanical energy harvesting and instantaneous motion sensor 1applications. Nano Energy, 74:104802. https://doi.org/10.1016/j.nanoen.2020.104802

Suphasorn, P., Appamato, I., Harnchana, V., Thongbai, P., Chanthad, C., Siriwong, C., and Amornkitbamrung, V.

(2021). Ag Nanoparticle-Incorporated Natural Rubber for Mechanical Energy Harvesting Application. Molecules, 26(9):2720. https://doi.org/10.3390/molecules26092720

Wang, H., Shi, M., Zhu, K., Su, Z., Cheng, X., Song, Y., Chen, X., Liao, Z., Zhang, M., and Zhang, H. (2016). High performance triboelectric nanogenerators with aligned carbon nanotubes. Nanoscale, 8(43):18489-18494. https://doi.org/10.1039/C6NR06319E

Wen, S., and Chung, D.D.L. (2001). Effect of admixtures on the dielectric constant of cement paste. Cement and Concrete Research, 31(4):673-677. https://doi.org/10.1016/S0008-8846(01)00475-6

Xin, C., Shifeng, H., Jun, C., and Zongjin, L. (2007). Piezoelectric, dielectric, and ferroelectric properties of 0-3 ceramic/cement composites. Journal of Applied Physics, 101(9):094110. https://doi.org/10.1063/1.2730559

Yoo, D., Go, E.Y., Choi, D., Lee, J.W., Song, I., Sim, J.Y., Hwang, W., and Kim, D.S. (2019). Increased interfacial area between dielectric layer and electrode of triboelectric nanogenerator toward robustness and boosted energy output. Nanomaterials, 9(1):71. https://doi.org/10.3390/nano9010071

Yu, A., Zhu, Y., Wang, W., and Zhai, J. (2019). Progress in triboelectric materials: Toward high performance and widespread applications. Advanced Functional Materials, 29(19):1900098. https://doi.org/10.1002/adfm.201900098

Yu, T.Y. (2011). Dielectric deamplification of multiphase cementitious composites in the frequency range of 0.5 GHz to 4.5 GHz. In Proceedings of 2011 Electrical Insulation Conference (EIC) (pp. 313-317). Annapolis, MD, USA. https://doi.org/10.1109/EIC.2011.5996169

Zhou, L., Liu, D., Wang, J., and Wang, Z.L. (2020). Triboelectric nanogenerators: Fundamental physics and potential applications. Friction, 8(3):481-506. https://doi.org/10.1007/s40544-020-0390-3